Han J. (2024) REAL-TIME MONITORING AND ANALYSIS OF ATHLETE MUSCLE ACTIVITY BASED ON WEARABLE SENSOR. Revista Internacional de Medicina y Ciencias de la Actividad Física y el Deporte vol. 24 (95) pp. 419-437
DOI: https://doi.org/10.15366/rimcafd2024.95.026

ORIGINAL

REAL-TIME MONITORING AND ANALYSIS OF ATHLETE MUSCLE ACTIVITY BASED ON WEARABLE SENSOR

Jilei Han

The Center for Physical Education, Xi'an Jiaotong University, Xi'an, Shaanxi, 710049, China.
E-mail: hjl13032932327@163.com

Recibido 20 de Junio de 2023 **Received** June 20, 2023
Aceptado 20 de Febrero de 2024 **Accepted** February 20, 2024

ABSTRACT

Muscle fatigue is a common phenomenon in life and work, which reduces work efficiency and quality of life, and also affects the performance of the biomechanical interface. It is of great research value to collect and analyze the information related to muscle contraction to study the mechanism of muscle fatigue. In order to better study the athlete muscle contraction movement, the principle of photoelectric volumetric tracing (PPG) to detect the athlete muscle contraction movement is introduced, and a reflective photoelectric muscle contraction sensing system that can detect four signals at the same time is designed. A programmable constant-current source is used to drive an infrared LED to irradiate infrared light into the muscle tissue, and the light transmitted out of the muscle is detected by another infrared detection circuit and converted into an electrical signal. Under the control of the microcontroller, the four detected electrical signals are time-conducted by analog multi-switches, followed by low-pass filtering and AD sampling, and finally the obtained four data are transmitted to the upper computer through the Bluetooth module for subsequent processing. The circuit realizes the synchronous detection function of 4-channel signals, and the system is accurate, reliable and has certain practical value.

KEYWORDS: Real-Time; Muscle Activity; Wearable Sensors

1. INTRODUCTION

The study of muscle movement state has good application value in the fields of clinical diagnosis, disease prevention and control, prosthetic control,

sports and daily health care. Muscle fatigue is a common phenomenon in life and work, which reduces work efficiency and quality of life, and also affects the performance of the biomechanical interface. It is of great research value to collect and analyze the information related to muscle contraction to study the mechanism of muscle fatigue. When muscle fatigue occurs, the ability of the muscle to generate force is reduced, which affects the coordination and flexibility of movement, thus reducing the quality of life and work efficiency. If the muscles cannot get reasonable rest after muscle fatigue occurs, it may even cause irreversible and serious damage to the muscles and make the corresponding parts of the human body lose the ability to continue working activities. If we can study the causes of muscle fatigue, find out the reasons for the decrease in muscle output capacity due to muscle fatigue as well as the reasons for the soreness of muscles, and have a comprehensive and clear understanding of muscle fatigue, we can detect the changes in the state information of the key muscles during the process of muscle fatigue, and arrange for a reasonable rest before the fatigue has a negative impact on the muscles and the human body to ensure that the working life has the highest efficiency and quality. For example, by collecting and detecting the muscle signals during the training process of athletes, deciphering the muscle state, and further obtaining the time nodes of muscle fatigue and other key information, so as to improve the training time plan, and arrange appropriate rest time when the athlete's muscles reach a certain state threshold, we can ensure that the athlete's long time to maximize the efficiency of training for daily training. Therefore, it is necessary to explore the mechanism of muscle fatigue.

Currently, surface electromyography (s EMG) and photo plethysmography (PPG) are commonly used in the study of muscle movement. Among them, surface electromyography is prone to electromagnetic interference and the electrodes in contact with the skin are susceptible to measurement errors due to sweating (Feng, Zhong, & Wang, 2014; C. Wu, Song, & Zeng, 2017), while photo plethysmography has the advantages of sensitive detection, immunity to electromagnetic interference, small size, low power consumption, etc. The surface electromyography and photo plethysmography methods have the same advantages. In the study of athlete muscle contraction movement using photoelectric volumetric tracing, the reflection method is mostly used, in which the light source and the sensor are located on the same side of the detection site. However, most of the reported research prototypes can only measure the state of one muscle at a time, and if the state of multiple muscles is to be detected, it can only be divided into multiple measurements. And most of the designs are designed with the light-emitting and light-detecting detection modules, as well as the microcontroller main control circuit, signal processing circuit and other modules all on one circuit board, so that the volume of the whole circuit system is relatively large, which is not conducive to wear on the body measurement. Based on the above shortcomings, this paper proposes an improvement program to design a

sensing circuit system that can detect multiple muscle movement states simultaneously, and separate the sensing part from other processing circuits, which improves the convenience of wearing the sensor.

2. Related Works

The advantage of the PPG method of heart rate measurement is that it utilizes the principle of photoelectric measurement, realizing non-invasive heart rate measurement without the need for human cooperation, which meets the demand for extracting the heart rate of the human body in life scenarios such as exercise and sleep. However, due to the inaccuracy of the variability of the heart rate extracted by this method, it is not possible to extract all the heart rate parameters. In terms of signal noise, the human body movement causes intermittent contact between the sensor and the wrist, resulting in time-varying motion artifacts mixed in the PPG signal, which increases the difficulty of heart rate extraction.

Kim proposed a method based on independent component analysis (ICA) to suppress the motion artifact component in the PPG spectrum, but the ICA method can only provide reliable output when the noise and information signals have mutually exclusive spectra (Kim & Yoo, 2006). Wu et al. used an adaptive filter based on recursive least squares to use the acceleration signal parallel to the direction of finger blood flow as a reference signal (C.-C. Wu, Chen, & Fang, 2017). Wenwen He et al. used the Volterra recursive least squares method to remove motion artifacts, which is novel in that it utilizes the nonlinear and memory effects of Volterra filters (Wenwen, 2021). However, the ANC method is very sensitive to the reference signal, and although the acceleration signal has a strong correlation with the motion noise, it does not fully characterize the change of the distance between the bracelet and the wrist, and thus can only remove some weak motion artifacts.

Pravaman et al. simultaneously acquired NIR spectral signals and EMG signals to determine the relationship between muscle oxygen metabolism and external forces (Praagman, Veeger, Chadwick, Colier, & Van Der Helm, 2003). It was demonstrated that NIR spectral signals can be used in musculoskeletal modeling studies. Boone and his team acquired EMG and NIR signals to investigate the relationship between physiological states (Boone, Barstow, Celie, Prieur, & Bourgois, 2015), such as muscle oxygenation, and pedal speed when performing high-intensity ramp exercise, and demonstrated that the joint acquisition and analysis of these two signals can yield more comprehensive and complementary information in the study of muscle movement. Taelman measured and analyzed various parameters derived from surface EMG signals and near-infrared spectroscopic signals and their relationship to muscle fatigue during static elbow flexion to exhaustion as well as during semi-dynamic exercise (Taelman et al., 2011). It was demonstrated that surface EMG signals

and NIR spectral signals provide additional information about muscle fatigue. Movahed et al. researchers recorded the relationship between the fatigue of the erector spinae muscle and the changes in the parameters related to the EMG signal and the NIR spectral signal under repetitive static contraction, and calculated the amplitude and median frequency of the EMG signal and the two types of hemoglobins. It was found that changes in median frequency were most closely related to fatigue sensation (Movahed, Ohashi, Kurustien, Izumi, & Kumashiro, 2011). In addition to the simultaneous acquisition and analysis of two signals to analyze fatigue, a relatively small number of studies have also acquired and analyzed three signals for the detection and analysis of muscle fatigue. Yoshitake and his team simultaneously acquired three signals, electromyography, near-infrared, and myoacoustics, from the lower back muscles of the subjects to study the fatigue mechanism of the lower back muscles (Yoshitake, Ue, Miyazaki, & Moritani, 2001). The aim was to explore the etiology of lower back muscle strain and to try to obtain information on lower back muscle fatigue from three aspects: electrophysiological, mechanical, and blood-oxygen metabolism.

3. Methodology

3.1 Near-infrared spectral signal

Near-infrared spectroscopic signals are collected by irradiating human tissue with near-infrared light whose wavelength is within the near-infrared spectral region. Non-invasive detection of tissue oxygen metabolism can be achieved using NIR spectroscopy. It has many advantages such as high efficiency, accuracy, convenience as well as no harm to the subject and no environmental hazards (Currà et al., 2019). There are four main characteristics of NIR spectroscopy irradiation of human muscle tissue:

(1) The human body is relatively transparent in the near-infrared spectral window of 650 to 1000 nm, with minimal reflection; (2) Chromophores in human tissues are capable of absorbing or scattering NIR light; (3) The propagation of the NIR spectrum in muscle tissue is mainly by scattering, and the typical value of the scattered intensity is usually 100 times higher than the absorbed intensity (Delpy & Cope, 1997); (4) Hemoglobin in small blood vessels located in the microcirculation is the main absorber of NIR light, while NIR spectroscopy is insensitive to blood vessels with a diameter greater than 1 mm (Ferrari & Quaresima, 2012).

Therefore, combined with the near-infrared spectrum irradiation of human tissue characteristics, due to the scattering effect of large, near-infrared light can be propagated through the human body tissue to the detector, the absorption intensity is mainly affected by the concentration of oxygen-containing and deoxygenated hemoglobin, in the case of the light source under

the condition of the constant total intensity of the light source, the reflection of the extremely weak, basically negligible, the intensity of the absorption of the concentration of oxygen with the blood to change, and further impact on the intensity of the scattered intensity, the metabolism of the oxygen for the changes in the blood in the small blood vessels can be very sensitively reflect the situation.

3.2 Sensing Principles

Muscles contain tissues such as epidermis, blood vessels, muscles and bones. When a beam of light is shone into a muscle, various substances in the blood absorb the light to varying degrees, and studies have shown that hemoglobin carried by red blood cells in the blood plays a major role in absorbing the light (Ward et al., 2006). Other light that is not absorbed undergoes transmission and scattering in the muscle, as shown in Figure 1. A portion of the scattered light will eventually exit the skin, presenting a curved transmission path (Han & Kim, 2009).

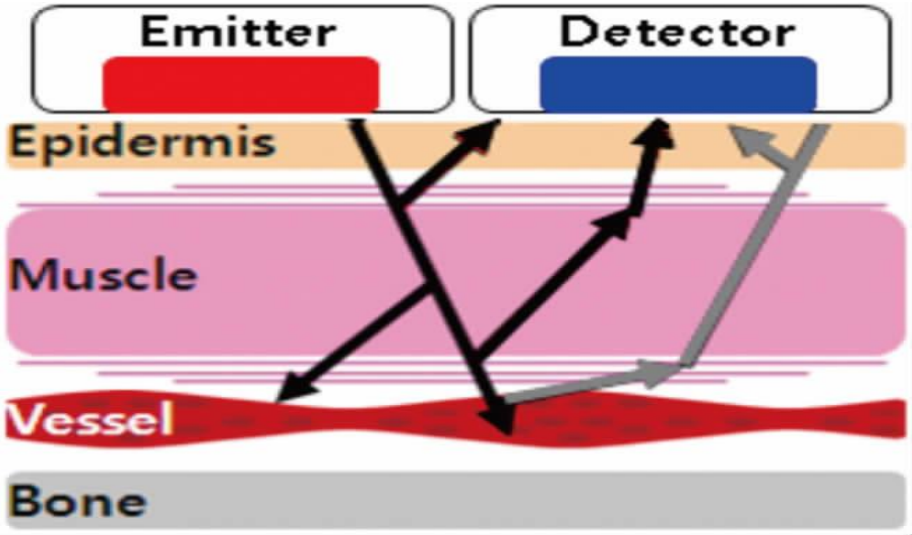

Figure 1: Transmission route of light in muscle tissue

When the muscle contraction, the muscle fibers in the muscle will become thicker, compression of blood vessels in the muscle, so that the blood flow is reduced, causing a decrease in the concentration of the main light-absorbing substance hemoglobin, which causes a decrease in the amount of absorbed light, the amount of light scattered out of the skin increases (Bianchi, Zambarbieri, Beltrami, & Verni, 1999), and the output of the photoelectric detection circuit outside the skin is correspondingly increased. This provides a basis for detecting the contraction state of the muscle.

3.3 Principles of NIR signal calculation

Changes in the concentration of absorbing substances cause changes

in the absorbed light intensity of the near-infrared signal, which leads to changes in the scattered light intensity received by the detector. In order to use the change in light intensity to invert the change in concentration of the absorbing substance, it is not enough to have a qualitative analysis, but a scientific quantitative relationship is needed to sustain it. The German mathematician Johann Lambert described the relationship between the degree of light absorption of a substance and the thickness of the medium in which the light can be absorbed in the substance, known as Lambert's law. The modified Lambert's Beer's law establishes the existence of a quantitative relationship between the intensity of absorbed light and the concentration of the light-absorbing substance.

The ratio of the intensity of light emitted through the tissue (transmitted light), I_1, to the intensity of incident light, I, is called the transmittance, T, and the formula can be expressed as:

$$T = \frac{I_1}{I} \qquad (1)$$

The greater the transmittance T, the weaker the absorption of light by the tissue, and conversely, the stronger the absorption, when the reflection is small. Take the negative logarithm of the transmittance, defined as the absorbance, the absorbance is expressed by A, the stronger the absorption of light by the tissue, the greater the absorbance A, the A formula is as follows:

$$A = -\ln T = \ln(I/I_1) \qquad (2)$$

Denoting the thickness of the light-transmitting tissue (in cm) by b and the scaling factor by k_1, Lambert's law is expressed as follows:

$$A = k_1 b \qquad (3)$$

Lambert's law emphasizes the relationship between tissue thickness and light absorption, and it applies to all homogeneous media. About a century later, the German physicist August Beer proposed that the strength of a tissue's ability to absorb light is also related to the concentration of light-absorbing substances. The proportionality coefficient of the concentration of the light-absorbing substance (determined by the nature of the substance to be measured, and the wavelength of the incident light) is expressed as k_2. C is the concentration of the amount of substance ($^{mol}/_{L}$). The specific form of Beer's law is:

$$A = k_2 C \qquad (4)$$

Beer's law is absolutely accurate when the incident light is a single

wavelength. Lambert's Beer's law can be summarized by analyzing the conclusions drawn from Lambert's and Beer's laws together against each other. When irradiated with a single wavelength of light, if the thickness of the tissue is fixed, there is a positive relationship between the A and the concentration of the light-absorbing substance, and this ratio is affected by the type of light-absorbing substance, the wavelength of the incident light, and the temperature of the tissue, as expressed in the following equation:

$$A = \varepsilon bC \qquad (5)$$

where ε is the molar absorption coefficient in $L \cdot mol^{-1} \cdot cm^{-1}$. If there is more than one light-absorbing substance in the tissue, as long as the coexisting substances do not reactively interact with each other, the absorbance of the tissue is the sum of the absorbance's of all the light-absorbing substances, with $A_a, A_b, A_c \cdots$ representing the absorbance of the light-absorbing substance $a, b, c \cdots$, i.e., there:

$$A = A_a + A_b + A_c + \cdots \qquad (6)$$

However, in actual measurements, deviations from Lambert's law are often found. This may be due to the complexity of the actual situation, where the incident beam is not guaranteed to be perpendicularly incident, the propagation path does not follow a straight line, but scatters along curved channels in the biological tissue, the actual propagation path is longer than the straight line distance, and the tissue conditions are not ideal as required by the law, which makes the accuracy of Lambert-Biel's law affected. Based on these influencing factors, the law was improved, culminating in a modified Lambert-Bill's law to fit the actual situation, with the following expression:

$$A = BL\varepsilon C + G \qquad (7)$$

Where L is the distance between the light source and the photodetector, B is the distance correction coefficient, and the product of B and L is the actual distance traveled by the light in the organization. The product of B and L is the actual distance traveled by the light in the tissue. In addition, the scattering attenuation of the light also affects the absorbance in actual measurements, so $G$is introduced as the scattering attenuation affecting factor. The modified Lambert's law is well adapted to the law of near-infrared light irradiation of human tissue.

However, the concentration of light-absorbing substances, C, cannot be solved from only one of the above equations. Therefore, let the light intensity received by the detector in the initial state of the tissue be I_0, and the light intensity received after the change of state be I_t, and the Lambert's Beer's law for the two states is subtracted to obtain the equation for the change of absorbance:

$$\Delta A = A(t) - A(0) = ln\left({I_0}/{I_t}\right) = BL\varepsilon\Delta C \qquad (8)$$

Eliminating the scattering attenuation factor G, the change in absorbance ΔA is obtained by calculating the light intensity measured by the photodetector by the following formula.

$$\Delta A = -ln\left({V_t - V_b}/{V_0 - V_b}\right) \qquad (9)$$

Where, V_0 and V_t are the initial voltage value measured by the detector and the voltage value after the change of state, respectively, and V_b is the voltage measured when the light source is not illuminated, the phase subtraction is intended to eliminate the interference of other noise. Therefore, the concentration change $\Delta C$of the absorbing substance can be obtained as long as the absorbing substance is determined with B and ε based on the properties of the absorbing substance.

For this study, however, there was not more than one light-absorbing substance in the tissue, and measuring and calculating the ΔC with only one wavelength of light only captured changes in the overall concentration of light-absorbing substances. The main light-absorbing substances in muscle tissue are oxygenated hemoglobin (HbO_2), deoxygenated hemoglobin (HHb), and cytochrome oxidase (Cyt-ox), and the metabolic profile of blood oxygenation is concerned with the change in concentration of the two types of hemoglobin, so that it is necessary to solve three equations by association. Therefore, for the measurement, three types of near-infrared light with different wavelengths are needed to obtain three Lambertian equations, as follows:

$$\begin{aligned}
\Delta A(\lambda_1) &= B(\lambda_1)L\left(\varepsilon_{HbO_2}^{\lambda_1}\Delta C_{HbO_2} + \varepsilon_{HHb}^{\lambda_1}\Delta C_{HHb} + \varepsilon_{Cyt-ox}^{\lambda_1}\Delta C_{Cyt-ox}\right) \\
\Delta A(\lambda_2) &= B(\lambda_2)L\left(\varepsilon_{HbO_2}^{\lambda_2}\Delta C_{HbO_2} + \varepsilon_{HHb}^{\lambda_2}\Delta C_{HHb} + \varepsilon_{Cyt-ox}^{\lambda_2}\Delta C_{Cyt-ox}\right) \\
\Delta A(\lambda_3) &= B(\lambda_3)L\left(\varepsilon_{HbO_2}^{\lambda_3}\Delta C_{HbO_2} + \varepsilon_{HHb}^{\lambda_3}\Delta C_{HHb} + \varepsilon_{Cyt-ox}^{\lambda_3}\Delta C_{Cyt-ox}\right) \qquad (10)
\end{aligned}$$

4. System Design

4.1 Selection and arrangement of light sources and detectors

The basic components for acquiring near-infrared spectral signals from muscle tissue are a near-infrared light source and a photodetector. For the NIR light source, it needs to be able to emit NIR light in three wavelengths. Two common NIR light sources are light-emitting diodes (LEDs) and lasers. The monochromatic nature of LEDs can make the results of blood oxygen metabolism calculations more accurate. And LED has the advantages of tiny

size, suitable price, high safety, and easy to use (Yadav, Rani, Singh, & Murari, 2014), so the NIR LED is chosen as the light-emitting light source. According to literature research (Wang, 2001), when one of the three near-infrared wavelengths is at 800 nm and the other two are separated around 800 nm, the calculation of blood oxygen metabolism by modified Lambert's Beer's law can well ensure the sensitivity of the light intensity change to the hemoglobin concentration. Therefore, the L4*730/4*805/4*850-40Q96-I near-infrared light source produced by Epitex was selected, which is cylindrical in shape and small in overall size, and is capable of emitting three kinds of near-infrared light at 730 nm, 805 nm and 850 nm, which is in line with the test requirements. For photodetectors, because the intensity of near-infrared light with the propagation distance attenuation, so propagation to the surface of the skin out of the light intensity is relatively weak, photodetectors must be able to detect the weak light intensity. TI integrated mutual impedance amplifier silicon photodiode OPT101 on the near-infrared spectral region of the light response is sensitive, linearity is good, its key parameters are shown in Table 1.

Table 1: Data sheet for OPT101

OPT101	**PARAMETER VALUE**
SUPPLY VOLTAGE (V)	2.7-36
DETECTOR SIZE (MM)	2.3□2.3
RESPONSIVENESS (A/W)	0.45
OUTPUT VOLTAGE (V/μW)	0.45
QUIESCENT CURRENT (μA)	120
NON-LINEARITY (% FULL SCALE OF BEST-FIT STRAIGHT LINE)	±0.01

The average power of the selected far wavelength of near-infrared light is 25mW, the response sensitivity of OPT101 is sufficient, and the range of supply voltage is large, which can be flexibly selected according to the conditioning circuit, the linearity is high, and the dark current and dark noise are both very small, and it is proved by the measurement that the photodetector can collect the stable and usable near-infrared spectral signal. After choosing a suitable light source and detector, the arrangement distance between the two needs to be considered. From the above principle, it can be seen that the detection depth of NIR light is about one-half of the distance from the detector to the NIR light source, and there are tissues such as skin and fat in the upper layer of the muscle, so if the detection depth is too small, it cannot accurately obtain the information of muscle contraction, so the distance between the NIR light source and the detector should not be too small. The thickness of the surface tissue is generally within 4 to 8 mm (Yamada et al., 2003). Therefore, the distance between the two should be more than 16mm. However, when the distance becomes larger, the scattered intensity of near-infrared light detected by the detector will decrease rapidly, and if the distance is too large, the light

intensity is too weak, which is also undesirable. Therefore, a distance greater than 16mm and not too far away should be chosen. Considering the arrangement of myoelectric electrode, microphone and the overall size, the distance between the detector and the light source is chosen to be 30mm.

4.2 Near-infrared spectral signaling circuit

The circuit of near-infrared spectral signal is divided into two parts, one is the near-infrared spectral signal generating circuit, and the other is the reception and conditioning of near-infrared spectral signal. For the near-infrared spectral signal generation circuit, according to the principle of blood oxygen metabolism calculation, the three wavelengths of near-infrared light far from the light can't be lit at the same time, so it needs to be driven and controlled by the driver chip. Select DM11A constant-current LED driver chip, the chip includes a shift register, data latch and constant-current circuit, with DAI, DCK, LAT, EN several control ports, the maximum output current value of the eight channels can be adjusted by an external resistor.

With the DM11A, the brightness of the three wavelengths of the near-infrared LED light source can be programmed and controlled. Located in the processing module of the microcontroller MSP430 in the near-infrared driver, through the DAI, DCK, LAT, EN ports for the DM11A input control commands, DM11A can be input for the LED light frequency and duty cycle of a specific pulse sequence to control the three wavelengths of the LED lights on and off in an orderly manner. For the reception and conditioning of near-infrared spectral signals, the near-infrared spectral signals collected by OPT101 also need to be filtered and amplified, and here the TLC277ID amplifier is selected. The schematic diagram of the near-infrared conditioning circuit, as shown in Figure 2.

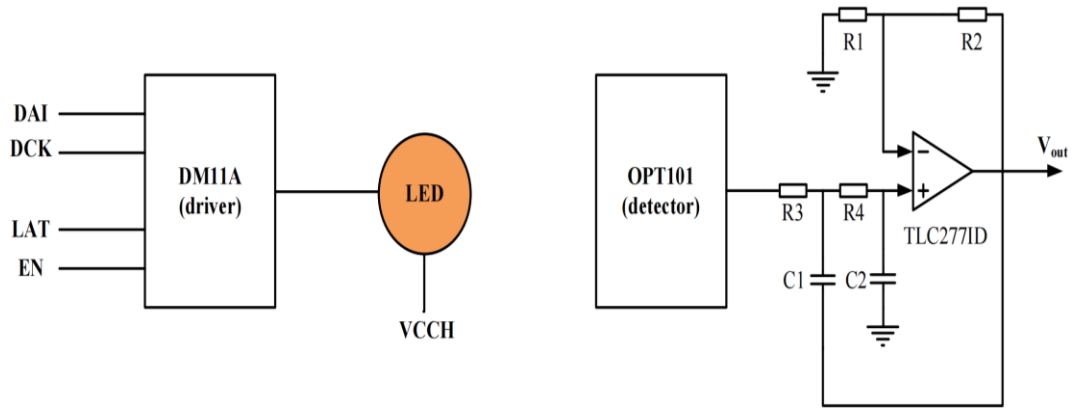

Figure 2: Schematic diagram of near infrared circuit

The amplified and filtered near-infrared spectral signal can be further transmitted to the host computer after analog-to-digital conversion by the subsequent processing module.

4.3 Selection of NIR light sources

The L4*730/4*805/4*850-40Q96-I near infrared light source is a cylinder with an outer diameter of 9mm and a height of 4mm, pin-type, with 8 pins. There are four groups of three-wavelength LEDs, the overall package is not small enough to replace the disassembly is very troublesome, due to the specificity of human tissue, a group of three-wavelength LED energy is enough to be OPT101 photodetector sensitive detection, so the choice of a large package of L4 * 730/4 * 805/4 * 850-40Q96-I is not necessary. Moreover, because of the thermal conductivity of the metal casing and the simultaneous operation of four sets of LEDs, it tends to heat up after a certain period of time. Although the driver adjusts the luminous time of the three wavelengths of LEDs to avoid the continuous emission of near-infrared lamps as much as possible, it may still get hot under long-term working conditions, which is unfavorable for wearing. Therefore, considering the needs of this experimental research and the compactness and convenience of the whole system, SMW760/810/840 are chosen to replace the original LEDs as the NIR light source. SMW760/810/840 are 3.2mm□2.7mm□1.8mm rectangular SMD NIR LEDs, as shown in Figure 3, possessing a set of three-wavelength light sources capable of emitting near-infrared (NIR) light at 760 nm, 810 nm, and 840 nm wavelengths. This meets the wavelength requirement of literature (Wang, 2001) to ensure the sensitivity of NIR light to hemoglobin. The package is small, the patch type is very convenient to disassemble, and it has its own transparent silicone lens, which ensures that the light source focuses the light, and there is no obvious hot phenomenon in long-time work, which meets the measurement requirements, and is better than the original near-infrared light source L4*730/4*805/4*850-40Q96-I.

Figure 3: Near-infrared light source SMW760/810/840

4.4 NIR light source and detector arrangement program

Although SMW760/810/840 is better than L4*730/4*805/4*850-40Q96-I in terms of volume package, ease of disassembly and heat generation, it also

brings another problem, which is that it is shorter than the photodetector due to its height of only 1.8mm, which makes it impossible for the NIR light source to be at the same height as the detector surface. If we use a translucent white shell, most of the NIR light will be conducted through the shell to the photodetector, rather than through the arc channel through the muscle tissue scattering into the OPT101, so the OPT101 is easily saturated, and cannot detect muscle oxygen metabolism; if we use a black light-absorbing shell, most of the NIR light is absorbed by the shell, and only a very small portion of the arc channel through the muscle tissue scattered into the detector, then the OPT101 will not get enough signal energy. If the black absorbing housing is used, most of the NIR light is absorbed by the housing and only a small portion is scattered into the detector through the curved channel through the muscle tissue. In addition, if the light source and the detector are in close proximity to the skin, the displacement and change of the contact surface caused by muscle contraction will seriously affect the accuracy of the NIR spectral signal. To address this problem, in the acquisition conditioning module for the near-infrared lamp and the detector to design a special light guide channel, placed near-infrared lamp from the other path to reach the detector, and the PCB version of the pin padding welding technology, padding the light source, so that it and the detector is the same height, the use of a black housing (to ensure that the detector receives all the light is after the light of the muscle tissue scattering), after you can Solve the problem of saturation or lack of energy. At the same time, the light guide channel strictly limits the height of the two positions, making the two surfaces 1.5mm away from the skin, so that the contact surface due to the contraction of the small changes caused by the NIR signal cannot be affected. After experimental verification, it was found that the 1.5mm non-contact measurement has no effect on the accuracy of the NIR signal and the accuracy of the concentration deduced by Lambert's law. After completion, the spacing between the LEDs and OPT101 is 29mm, as shown in Figure 4.

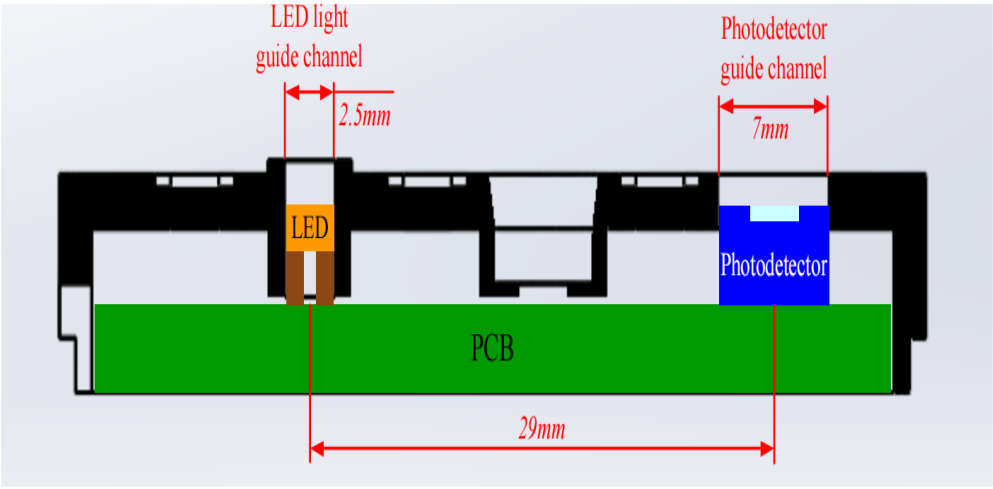

Figure 4: Near-infrared light guide channel (sectional drawing)

4.5 Multiple Switching and Filtering Circuits

The infrared detection signals from the 4 channels are then sent to the 4 inputs of the analog multi switch chip 74LV4051 as shown in Figure 5. Under the control of the microcontroller, the multi switch conducts only one signal at a time to the succeeding second-order Butterworth low-pass filter to filter out high-frequency noise interference. After filtering, the signal is amplified in phase and then sent to the 10-bit ADC sampling port that comes with the ATmega48 microcontroller to be converted to a digital signal.

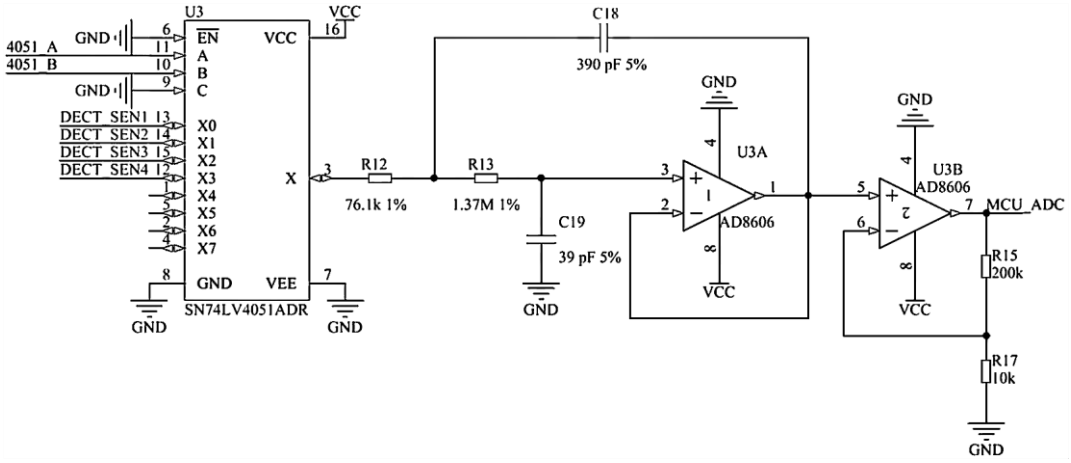

Figure 5: Multi-switching and low-pass filtering circuits

4.6 Microcontroller and Peripheral Circuits

The main control microcontroller and peripheral circuits are shown in Figure 6, and the ATmega48 microcontroller from Microchip is selected, which is a low-power CMOS microcontroller with enhanced RISC architecture and rich on-chip resources. It integrates the I2C bus control module, 10-bit ADC sampling module, timers, counters, etc. required for the control of the aforementioned DAC chip LTC2635-LZ8. The microcontroller is connected to the HC42 low-power Bluetooth module through the internal USART serial transmission module, and sends the sampled 10-bit digital signal in 2byte to the upper computer side for processing at a baud rate of 57600bit/s.

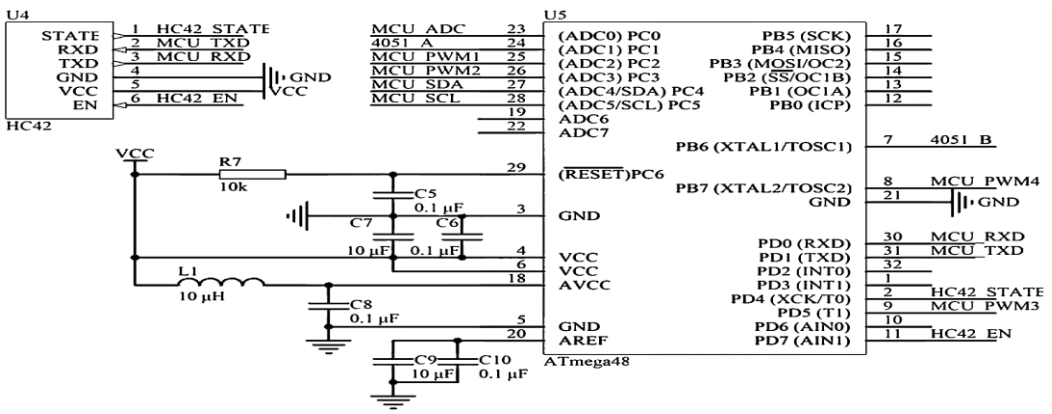

Figure 6: Microcontroller and Peripheral Circuit

5. System Debugging

5.1 Dark noise and drift in NIR signals

For NIR signals, their dark noise and drift are selected as evaluation metrics. Dark noise and drift are commonly used evaluation metrics for optical sensors. Dark noise is the noise signal detected when the spectral sensor is in a dark room without light (i.e., when there is no light input to the detector). It is a kind of noise inside the optical sensor, especially the detector, which affects the spectral raw data.

Prior to testing the dark noise, the program in the processing module microcontroller was set to change so that the NIR LEDs did not emit light and were off the entire time. Place the muscle sensing system in a black box in the darkroom. Activate the sensing system and record the signal received by the photodetector for 1 hour.

Dark noise usually consists of two components, direct flow, which is reflected by calculating the mean value of the data received by the photodetector, and fluctuation, which is reflected by the variance of the 1-hour data. Calculated data, in 1 hour, the average value of photodetector of two channels are 27.35m V and 28.17m V, and the variance is 0.66m V and 0.73m V. The direct flow is below 30m V, which is not much effect on the NIR signals, and it can be eliminated by the software of the upper computer.

And the fluctuation is very weak and negligible for the NIR signal, the dark noise experiment is passed. Sensor drift is the change in output over time when the signal input to the sensor remains constant. It usually comes from the noise of the sensing system itself and from the external environment. Because drift is strongly influenced by the test conditions, to test the drift of the NIR part it is best to restore the conditions of the subsequent exploration experiments.

Testing for drift requires the acquisition of NIR signal data over a long period of time, and if worn on the human body it is easy to incorporate other influences than simple drift, so it is necessary to find a static prosthesis that can mimic human tissue.

In order to avoid confusion in the calculation of the three wavelengths of NIR light, the NIR driver in the microcontroller of the processing module was changed to one kind of LED intervals to light on and off, and the LEDs of the other two wavelengths were in the state of being off. The sensing system was fixed to the static calibration prosthesis with double-sided adhesive (the same way as in the test of real muscles) and put into the dark room black box.

Each wavelength of near-infrared light was collected for one hour, for a

total of three hours to complete the experiment. After obtaining the data, the average value of the data obtained from the three wavelengths is obtained, and the maximum and minimum values are taken out to make a difference, and the difference is compared with the average value, which is used as the drift of this wavelength in the near infrared. The results are shown in Table 2.

Table 2: Drift of near infrared lights with three wavelengths

NEAR INFRARED WAVELENGTH (NM)	760	810	840
AVERAGE VALUE (V)	1.01	1.36	1.51
SENSOR DRIFT	0.12%	0.12%	0.15%

From the results, it can be seen that the maximum drift for the three wavelengths is only 0.15% at 840nm. The accuracy is able to meet the needs of the research objectives of this paper.

6. System Testing and Discussion

6.1 System Testing

The upper limb muscle groups of the dumbbell bending movement were measured by wearable sensors. The LED driving current of the four channels was set at 80 mA, and four sensing modules were placed on the radial wrist flexor of the forearm, the deltoid muscle of the shoulder, the biceps and triceps muscles of the upper arm, and the sensing modules were connected to the main control board of the microcontroller with a row of wires.

Holding a 2kg dumbbell in hand, the arm was naturally lowered at first, and then keeping the upper arm fixed, the elbow joint was used as the pivot point of the forearm to slowly bend upward to the highest point, and then slowly put down.

The collected 4-channel data were plotted into a curve graph with MATLAB software, as shown in Figure 7. In the graph, the horizontal axis indicates the number of sampling points, sampling once every 10ms, a total of 1500 data sampling, time 15s, the vertical axis indicates the sampling voltage value.

From the figure, it can be seen that the acquired curve has burr interference, in order to eliminate the burr, the data are subjected to sliding average filtering, as shown in Equation (11), and the sliding window is taken 8 data points at a time. The curve after the sliding average is shown in Figure 8, and the curve becomes much smoother.

$$Y(n) = \frac{1}{N}[X(n) + X(n-1) + \cdots + X(n-N+1)] \qquad (11)$$

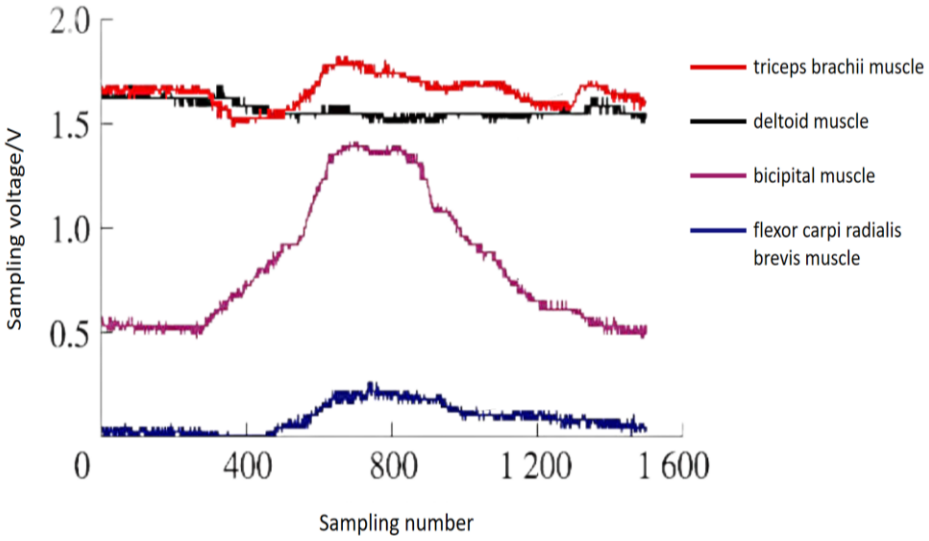

Figure 7: Raw measurement data curve

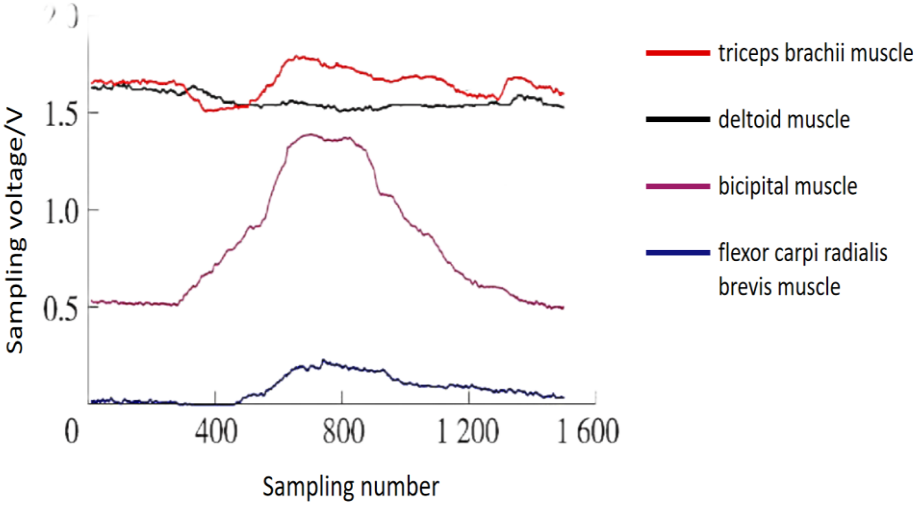

Figure 8: Measurement curve after slide averaging

6.2 Discussion

From the measurement results, it is seen that the circuit system using wearable sensors realizes the function of detecting 4-channel muscle contraction states simultaneously, and the changes in the data curve reflect the changes in the degree of contraction of the muscle group at the same time. The burr interference on the initial curve is well eliminated after the sliding average filtering process and the curve becomes smooth.

From the measurement curves, the upper arm biceps brachii and forearm radial wrist flexor changed significantly. At the very beginning when the arm was naturally lowered, these 2 muscles were basically in a relaxed state, so the detected voltage was low. As the forearm was bent upward to its highest point, there was a significant increase in both of these 2 curves, with the biceps brachii showing the most pronounced change in curve, with an elevation of

about 1V. As the dumbbell is lowered, these 2 curves slowly fall back down to near their initial values. The reason the triceps and deltoid muscles have a higher starting voltage when the arm is lowered is that when the dumbbell is hand-held, these two muscles are initially in a state of applied force contraction. As seen in Figure 10, there is a slight descent and then elevation of the triceps during the lifting of the dumbbell and, conversely, a slight elevation and then descent during the lowering of the dumbbell. The elevation or descent was synchronized with the elevation or descent of the biceps and radial wrist flexor curves. This means that as the dumbbells are lifted, the biceps and radial wrist flexors contract, while the triceps muscle is slightly stretched and then significantly contracted, and the opposite process occurs when the dumbbells are lowered. The change in state of the triceps brachii was carefully observed during the actual movement and is indeed shown in the curve. As can be seen, the 4-way data curve is well synchronized to reflect the changes in the state of stretching and contraction of the muscle group, and small changes can also be detected.

7. Conclusion

Normal human activities are closely related to muscle contraction, and muscle contraction is accompanied by a variety of physiological phenomena, the collection and interpretation of athlete muscle contraction movement information can help people understand the physiological mechanisms of muscle contraction, and can also be applied to achieve further output control. On the one hand, among the physiological phenomena related to muscle contraction, muscle fatigue is very common, and it is important to explore and master the deeper mechanism of muscle fatigue to prevent muscle fatigue, rationalize working time and improve work efficiency. However, when collecting and interpreting muscle contraction information to study muscle fatigue, only collecting and analyzing one kind of signal is incomplete and inaccurate, and there is no way to clearly and comprehensively understand the mechanism of muscle fatigue process. This paper describes the principle of detecting athlete muscle contraction movement using wearable sensors, and designs a muscle contraction sensing circuit system that can measure 4 signals simultaneously. The design of the circuit to detect 4 signals simultaneously is a functional improvement of similar circuits. The 4 sensing modules in the circuit are placed separately from the main control module of the microcontroller, which increases the wear ability of the whole circuit system. From the test results, the circuit system is accurate in measurement, stable in operation, realizes the expected function, and has certain practical value.

Reference

Bianchi, T., Zambarbieri, D., Beltrami, G., & Verni, G. (1999). NIRS monitoring of muscle contraction to control a prosthetic device. In *Biomedical*

Sensors, Fibers, and Optical Delivery Systems (Vol. 3570, pp. 157-163): SPIE.

Boone, J., Barstow, T. J., Celie, B., Prieur, F., & Bourgois, J. (2015). The impact of pedal rate on muscle oxygenation, muscle activation and whole-body VO 2 during ramp exercise in healthy subjects. *European journal of applied physiology, 115*, 57-70.

Currà, A., Gasbarrone, R., Cardillo, A., Trompetto, C., Fattapposta, F., Pierelli, F., . . . Serranti, S. (2019). Near-infrared spectroscopy as a tool for in vivo analysis of human muscles. *Scientific reports, 9*(1), 8623.

Delpy, D., & Cope, M. (1997). Quantification in tissue near–infrared spectroscopy. *Philosophical transactions of the royal society of London. Series B: Biological Sciences, 352*(1354), 649-659.

Feng, Y., Zhong, X., & Wang, J. (2014). DSP-based electromyographic signal acquisition and processing. *Electronic Device, 37*(5), 830-834.

Ferrari, M., & Quaresima, V. (2012). A brief review on the history of human functional near-infrared spectroscopy (fNIRS) development and fields of application. *NeuroImage, 63*(2), 921-935.

Han, H., & Kim, J. (2009). Novel muscle activation sensors for estimating of upper limb motion intention. In *2009 Annual International Conference of the Ieee Engineering in Medicine and Biology Society* (pp. 3767-3770): IEEE.

Kim, B. S., & Yoo, S. K. (2006). Motion artifact reduction in photoplethysmography using independent component analysis. *IEEE Transactions on Biomedical Engineering, 53*(3), 566-568.

Movahed, M., Ohashi, J.-y., Kurustien, N., Izumi, H., & Kumashiro, M. (2011). Fatigue sensation, electromyographical and hemodynamic changes of low back muscles during repeated static contraction. *European journal of applied physiology, 111*, 459-467.

Praagman, M., Veeger, H., Chadwick, E., Colier, W., & Van Der Helm, F. (2003). Muscle oxygen consumption, determined by NIRS, in relation to external force and EMG. *Journal of biomechanics, 36*(7), 905-912.

Taelman, J., Vanderhaegen, J., Robijns, M., Naulaers, G., Spaepen, A., & Van Huffel, S. (2011). Estimation of muscle fatigue using surface electromyography and near-infrared spectroscopy. In *Oxygen transport to tissue XXXII* (pp. 353-359): Springer.

Wang, Y.-q. (2001). Theory and technology of nondestructive measurement for biological tissue optical properties. *Optical Technique, 27*(4; ISSU 150), 355-382.

Ward, K. R., Ivatury, R. R., Barbee, R. W., Terner, J., Pittman, R., Torres Filho, I. P., & Spiess, B. (2006). Near infrared spectroscopy for evaluation of the trauma patient: a technology review. *Resuscitation, 68*(1), 27-44.

Wenwen, H. (2021). *Research on physiological signal analysis and processing algorithms for wearable devices*: University of Electronic Science and Technology.

Wu, C.-C., Chen, I.-W., & Fang, W.-C. (2017). An implementation of motion artifacts elimination for PPG signal processing based on recursive least squares adaptive filter. In *2017 IEEE biomedical circuits and systems conference (BioCAS)* (pp. 1-4): IEEE.

Wu, C., Song, A., & Zeng, H. (2017). Hand output force estimation based on s EMG and GRNN. *Journal of Instrumentation, 38*(1), 97-104.

Yadav, J., Rani, A., Singh, V., & Murari, B. M. (2014). Near-infrared LED based non-invasive blood glucose sensor. In *2014 International Conference on Signal Processing and Integrated Networks (SPIN)* (pp. 591-594): IEEE.

Yamada, E., Kusaka, T., Miyamoto, K., Tanaka, S., Morita, S., Tanaka, S., . . . Itoh, S. (2003). Relationships between changes in oxygenation during exercise and recovery in trained athletes. *Optical review, 10*, 436-439.

Yoshitake, Y., Ue, H., Miyazaki, M., & Moritani, T. (2001). Assessment of lower-back muscle fatigue using electromyography, mechanomyography, and near-infrared spectroscopy. *European journal of applied physiology, 84*, 174-179.